Jam phases in a two-dimensional cellular-automaton model of traffic flow

Shin-ichi Tadaki*
Department of Information Science, Saga University, Saga 840, Japan

Macoto Kikuchi†
Department of Physics, Osaka University, Toyonaka 560, Japan
(Received 17 November 1993; revised manuscript received 27 May 1994)

The jam phases in a two-dimensional cellular-automaton model of traffic flow are investigated by computer simulations. Two different types of jam phases are found. The spatially diagonal long-range correlation obeys a power law at the low-density jam configurations. The diagonal correlation exponentially decays at the high-density jam. The exponent of the short-range correlation in the diagonal direction is introduced to define the transition between these two phases. We also discuss the stability of the jams.

PACS number(s): 05.70.Ln, 64.60.Cn, 89.40.+k

I. INTRODUCTION

The investigation of traffic flow has been based mainly on the methods of fluid dynamics. For example, it has been studied with the Burgers equation in one-dimensional cases. Many attempts have been made to apply cellular-automaton modeling to fluids for computational simplicity. In recent years, considerable interest has developed also in the cellular-automaton modeling of traffic flow. One of the simplest models of traffic flow in one-way expressways is the rule-184 elementary cellular-automaton [1], which is a simple asymmetric exclusion rule. In spite of the simplicity of the model, it shows a phase transition from a freely moving phase at low vehicle density to a jamming phase at high vehicle density. More realistic models considering a variety of speeds of cars and effects of blockages have been investigated in one-dimensional models [2–5]. $1/f$ fluctuation has been observed in both actual expressways [6] and models [3,7].

Two-dimensional cellular-automaton models, however, have fewer direct connections to real traffic flow problems. They seem to be abstract models for a traffic system in a whole city or an expressway network. One of the simplest two-dimensional traffic models has been investigated by Biham, Middleton, and Levine (BML) [8]. They found a sharp transition between a freely moving phase at low vehicle density and a jamming phase at high density. The model has been extended to take into account the probability of changing directions of cars [9]. Nagatani has studied the effect of a traffic accident or a stagnant street on the growth of traffic jams [10,11]. He has also investigated the model with two-level crossings [12].

These studies with cellular-automaton models have not concerned only the actual traffic problems or traffic light controls; attention has also been paid to the phase transitions and the self-organized behaviors in such simple systems. Most works have investigated the phase transition of the system. However, few have paid attention to the structure and stability of jam configurations.

In this paper we are interested mainly in the spatial correlation in the jamming phase of the BML model, a simple model for two-dimensional traffic flow, where cars are represented as right and up arrows exclusively distributed on a square lattice and controlled by a traffic light. As will be seen in later sections, there are two types of jam phases. We discuss the spatial correlations of these two phases and define the transition point. We also discuss the stability of the jams in both phases.

This paper is organized as follows. We describe the BML model in Sec. II, where the occurrence of the phase transition from the freely moving phase to the jam phase is mentioned as well. Spatial correlations in the jam phases are discussed in Sec. III. In Sec. IV we investigate the diagonal correlations. The transition point between two types of jam is defined using short-range correlation. The stability of the jam configurations is studied by applying a perturbation which disturbs the jam configuration in Sec V. The distribution of the lasting time of perturbations is discussed. Section IV is devoted to summary and discussion.

II. MODEL

The model we study is the same as model I of Biham, Middleton, and Levine [8]. Cars are distributed on a square lattice of $N \times N$ sites with periodic boundary conditions in both horizontal and vertical directions. Each car is represented as an arrow directed up or right. The model is, therefore, a three-state cellular automaton with empty sites, up-directed, and right-directed cars as inner states of each site. A traffic light controls the dynamics, such that the right arrows move only at odd time steps

*Electronic address: tadaki@ai.is.saga-u.ac.jp
†Electronic address: kikuchi@godzilla.phys.sci.osaka-u.ac.jp

and the up arrows move at even time steps. (In the original BML model, right arrows move at even steps and up ones at odd steps.) At odd time steps, each right arrow moves one site to its right neighborhood if and only if the destination is empty. The corresponding rule is applied for up arrows. The dynamics and the periodic boundary conditions guarantee the conservation of the number of cars for each column and row; there are $2N$ conservation rules.

The density of right (up) cars is given by

$$p_{\rightarrow} = \frac{n_{\rightarrow}}{N^2}, \tag{2.1}$$

$$p_{\uparrow} = \frac{n_{\uparrow}}{N^2}, \tag{2.2}$$

where $n_{\rightarrow}$ ($n_{\uparrow}$) denotes the number of right (up) arrows. We examine the isotropic case where $p_{\rightarrow} = p_{\uparrow} = p/2$ following Biham, Middleton, and Levine. They reported the existence of the transition point $p = p_c \sim 0.35$. (Nagatani has investigated the transition point to be just under 0.4 in the large system limit $N \rightarrow \infty$ [13].) Below the transition point, all cars move freely and the average velocity is $\overline{v} = 1$. All cars are blocked and the average velocity vanishes above the transition point. Such a sharp transition occurs because the right and up arrows block each other. That is in contrast with one-dimensional models, where the average velocity goes down to zero gradually with increasing density above the transition point. In the following sections we show results of the $N = 128$ simulations.

III. TWO TYPES OF TRAFFIC JAM

Two types of traffic jam configurations are found in the BML model through the simulation. Figures 1 and 2 show typical traffic jam configurations. We investigate the structures, especially the spatial correlations, of these two configurations.

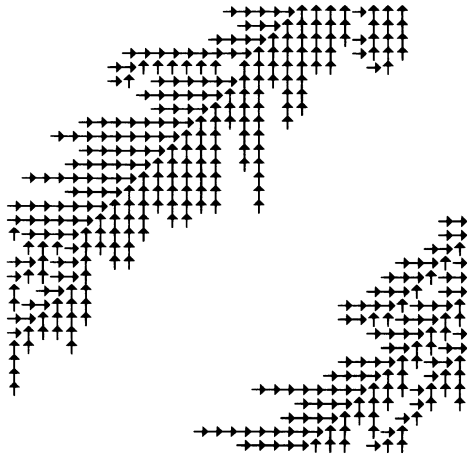

FIG. 1. A typical jamming configuration in the low-density region above the transition p_c. The global cluster of the jam is oriented diagonally. The system size is 32×32 and the density $p = 408/(32 \times 32) \sim 0.4$.

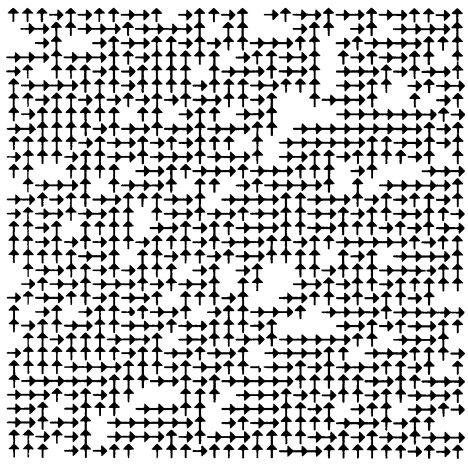

FIG. 2. A typical jamming configuration in the high-density region above the transition p_c. The system is covered by local clusters of the jam. The system size is 32×32 and the density $p = 920/(32 \times 32) \sim 0.9$.

In the low-density region, a single global cluster of jam is oriented from the lower-left corner to the upper-right one. The backbone of the jam lies diagonally and branches of the jam spread horizontally and vertically like a herringbone. It takes a long time to reach the jam state starting from random initial configurations. So the jam state at the low density is far from random configuration and well self-organized. The situation seems to have similarity with traffic jams caused by traffic accidents in the countryside.

In the high-density region, on the other hand, patches of small local clusters of jam cover the whole system. There is no apparent global structure. Starting from random initial configurations, it needs only a short time to get all cars stopped. Thus randomness initially given is expected to remain. This type of configuration seems to model chronic traffic jams in big cities. An escape from a jam only means catching up to the tail of another jam in such a situation.

We investigate spatial correlation functions to study more detailed characteristics of jam configurations. We first define the distribution function of right-directed (up-directed) cars:

$$\rho_d(\vec{r}) = \sum_i \delta(\vec{r} - \vec{R}_{d,i}), \tag{3.1}$$

where $d = \rightarrow$ or $\uparrow$ denotes the direction and

$$\delta(x) = \begin{cases} 1, & x = 0, \\ 0 & \text{otherwise.} \end{cases} \tag{3.2}$$

The coordinates $\vec{R}_{\rightarrow,i}$ ($\vec{R}_{\uparrow,i}$) are those of the ith right (up) car. The correlation functions are defined as

$$C_{dd'}(\vec{r}) = \frac{1}{n_d} \left\langle \sum_{\vec{x}} \rho_d(\vec{x}) \rho_{d'}(\vec{x} + \vec{r}) \right\rangle . \tag{3.3}$$

The symbol $\langle\,\rangle$ denotes the sample average, namely, the average over the jam configurations starting from different random initial configurations. The correlation function $C_{dd'}(\vec{r})$, therefore, stands for the probability to find a d'-directed arrow at the relative position $\vec{r}$ from a d-directed arrow. If the correlation between the same directed cars vanishes, $C_{dd}(\vec{r})$ goes down to the density p_d ($\vec{r} \neq 0$). We also define the *normalized* correlation function

$$\tilde{C}_{dd}(\vec{r}) = \frac{C_{dd}(\vec{r}) - p_d}{1 - p_d}. \tag{3.4}$$

The contour maps of the normalized correlation functions $\tilde{C}_{dd}(\vec{r})$ are shown in Figs. 3, 4, and 5. At low density (Fig. 3), the correlation spreads diagonally over the system size. The diagonally spreading spatial correlation corresponds to the jam structure shown in Fig. 1. Increase of the density weakens the diagonal correlation. The strong diagonal correlation still remains at intermediate density (Fig. 4). The decay of the diagonal correlation causes vibration in the antidiagonal direction. At high density (Fig. 5), at last, the correlation is suppressed, reflecting randomness.

IV. DEFINING THE TRANSITION POINT

The spatial correlation in the diagonal direction seems to be a key to characterize the two types of jams. The diagonal correlation $\tilde{C}_{dd}^{\mathrm{diag}}(r)$ is defined as the spatial correlation $\tilde{C}_{dd}(\vec{z})$ between diagonally separated arrows with the relative position $\vec{z} = r(\hat{x} + \hat{y})$, where the circumflex identifies a unit vector. In the low-density jam, one can find that the diagonal correlation obeys a power law (Fig. 6). In the high-density jam, the long-range diagonal correlation dies out more rapidly than a power law (Fig. 7).

We investigate the exponent of the power law in the diagonal correlation. It can be estimated easily for the low-density jam as

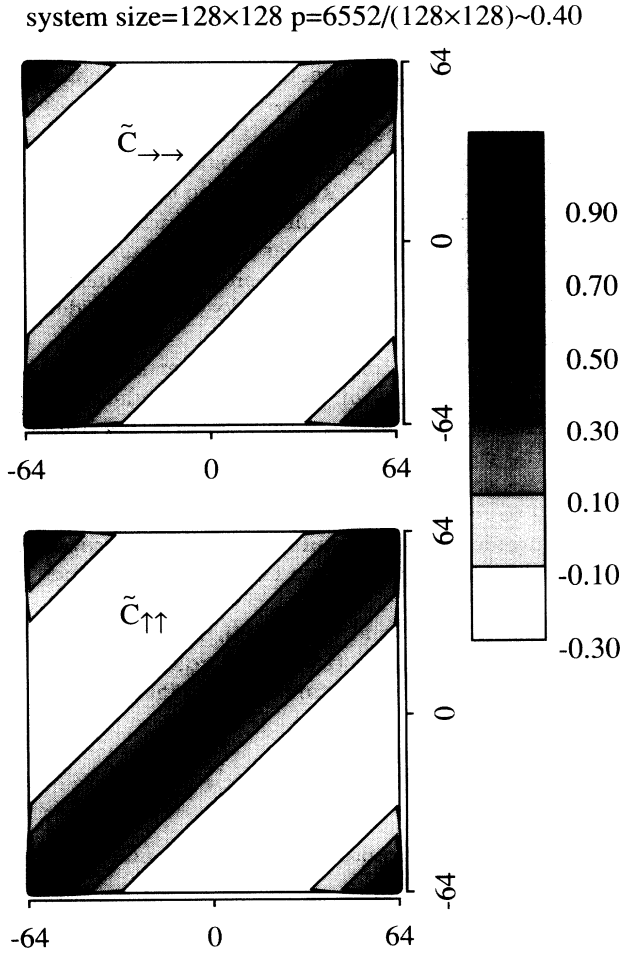

FIG. 3. The normalized correlation functions $\tilde{C}_{dd}(\vec{r})$ at low density. The upper diagram is of $\tilde{C}_{\rightarrow\rightarrow}(\vec{r})$ and the lower $\tilde{C}_{\uparrow\uparrow}(\vec{r})$. The correlation spreads diagonally over the system size. The high-value regions at the upper-left and lower-right corners are caused by finite-size effects. The system size is 128×128 and the density $p = 6552/(128 \times 128) \sim 0.4$. The average is taken over ten samples.

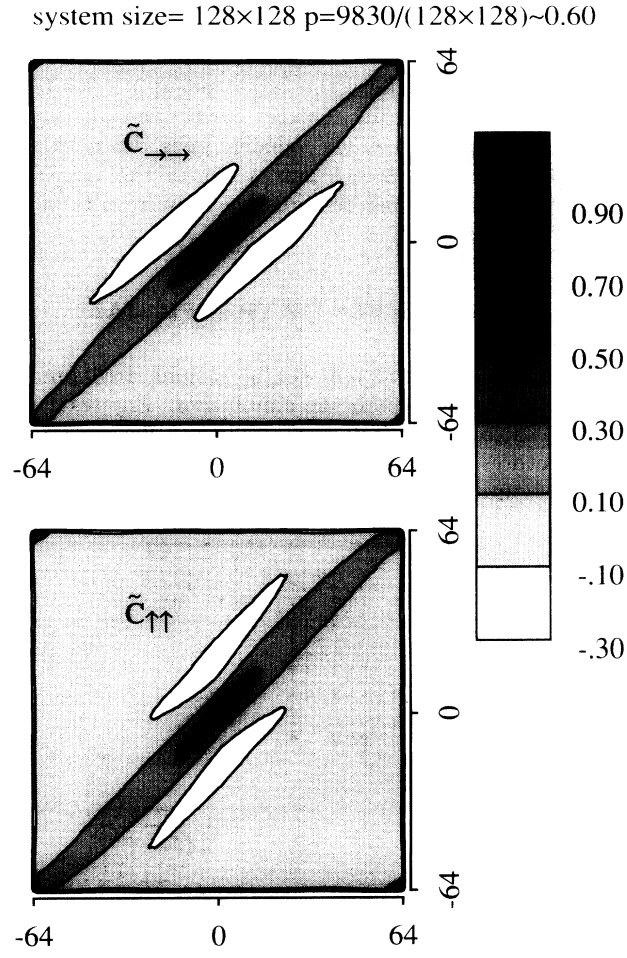

FIG. 4. The normalized correlation functions $\tilde{C}_{dd}(\vec{r})$ at intermediate density. The upper diagram is of $\tilde{C}_{\rightarrow\rightarrow}(\vec{r})$ and the lower $\tilde{C}_{\uparrow\uparrow}(\vec{r})$. The correlation mainly spreads diagonally over the system size. There appears a vibration in the antidiagonal direction in contrast to the low-density jam. The system size is 128×128 and $p = 6552/(128 \times 128) \sim 0.4$. The average is taken over ten samples.

$$\tilde{C}_{dd}^{\mathrm{diag}}(r) \sim r^{-\beta}, \quad \beta \sim 0.1. \tag{4.1}$$

On the other hand, the correlation in the high-density jam does not obey a power law. So we approximate the short-range correlation of the power law and define an effective exponent for the high-density jam. Actually we fit the short-range data $[\log_{10} r, \log_{10} \tilde{C}_{dd}^{\mathrm{diag}}(r)]$ $(1 \le r \le n < N/2)$ to a linear function by the method of least squares. Namely, parameters β and γ are chosen to minimize the squared deviation

$$\chi_n(\beta,\gamma)^2 = \sum_{r=1}^{n} [\log_{10} \tilde{C}_{dd}^{\mathrm{diag}}(r) - \beta \log_{10} r - \gamma]^2, \tag{4.2}$$

for fixed n. Then we maximize the range n under the condition

$$\left(\frac{1}{n} \min \chi_n(\beta,\gamma)^2\right)^{1/2} < \epsilon, \tag{4.3}$$

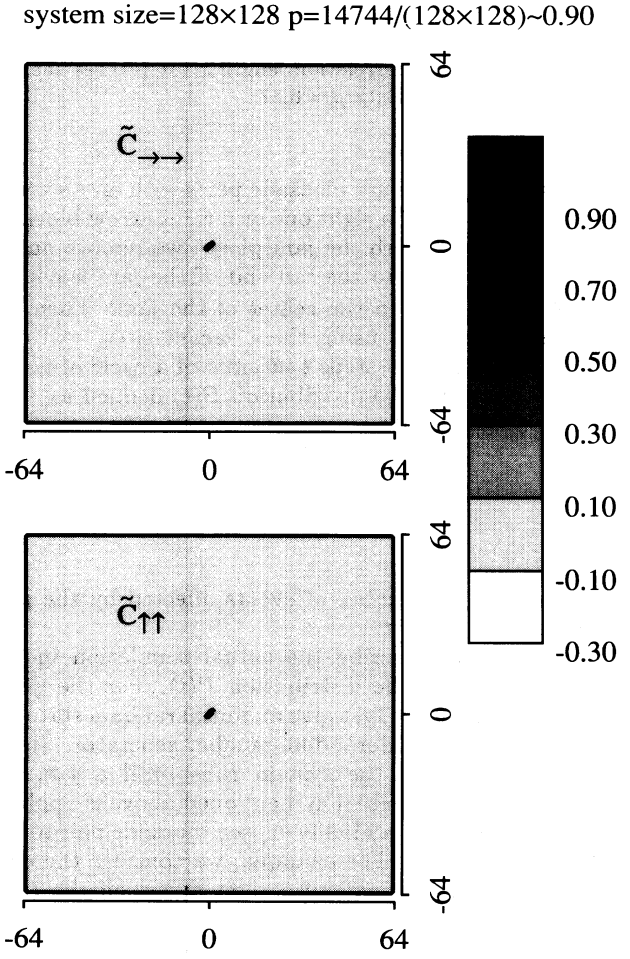

FIG. 5. The normalized correlation functions $\tilde{C}_{dd}(\vec{r})$ at high density. The upper diagram is of $\tilde{C}_{\rightarrow\rightarrow}(\vec{r})$ and the lower $\tilde{C}_{\uparrow\uparrow}(\vec{r})$. The values of $\tilde{C}_{dd}(\vec{r})$ are almost zero over the whole region except in the vicinity of the coordinate origin. The system size is 128×128 and $p = 14744/(128 \times 128) \sim 0.9$. The average is taken over ten samples.

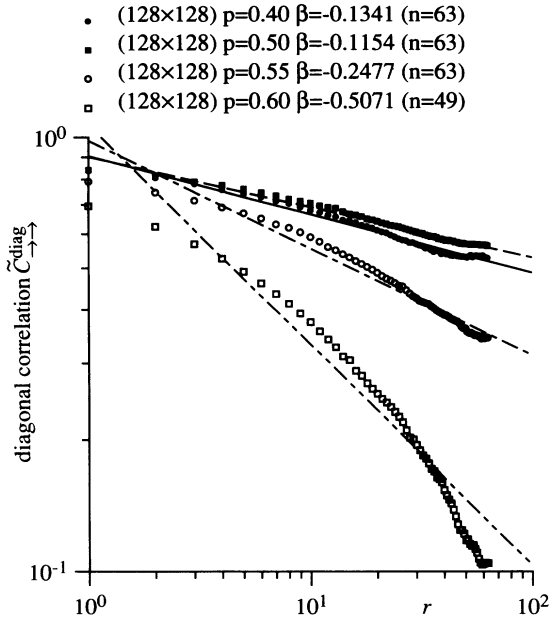

FIG. 6. The diagonal correlation $\tilde{C}_{\rightarrow\rightarrow}^{\mathrm{diag}}(r)$, the normalized correlation between right arrows separated diagonally by the distance $2^{1/2}r$, is plotted for $p \le 0.6$. The average is taken over 10 samples as in Figs. 3 and 5. The lines are fitted with the method of least squares with $\epsilon = 0.05$ in Eq. (4.3).

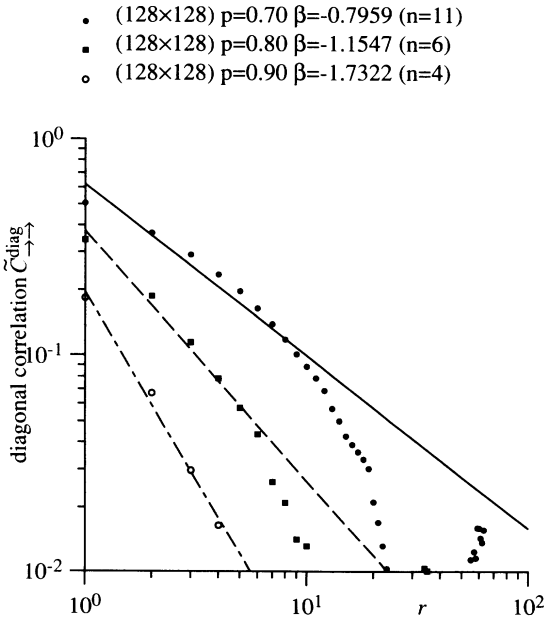

FIG. 7. The diagonal correlation $\tilde{C}_{\rightarrow\rightarrow}^{\mathrm{diag}}(r)$, the normalized correlation between right arrows separated diagonally by the distance $2^{1/2}r$, is plotted for $p \ge 0.6$. The average is taken over ten samples as in Figs. 3 and 5. The lines are fitted with the method of least squares for small r with $\epsilon = 0.05$ in Eq. (4.3).

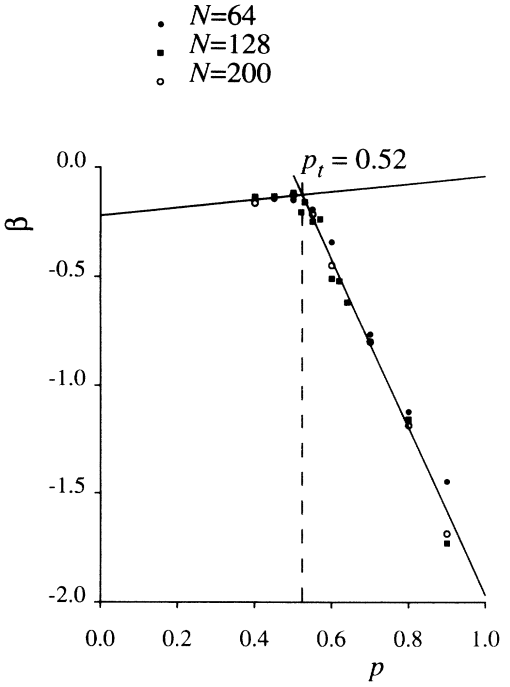

FIG. 8. Dependence of the exponents β on the density p.

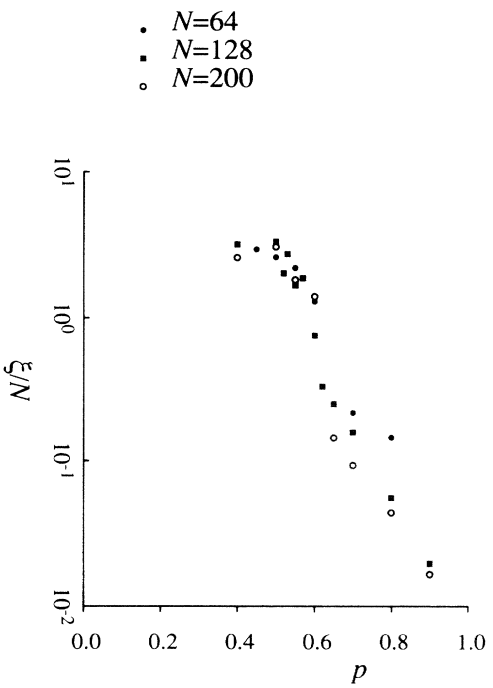

FIG. 9. Diagonal correlation length ξ. It reaches the system size N at the density $p = 0.57$.

where ϵ is an adequate constant, which all data in the low-density phase are fitted with.

Figure 8 shows the dependence of the exponent β on the density p for $N = 64$, 128, and 200 systems. One can find a clear transition between low-density and high-density regions at $p_t = p \sim 0.52$. The low-density jam above the transition point p_c, namely, $p_c < p < p_t$, shows a power-law diagonal correlation. The exponent of the correlation is $\beta \sim 0.1$. In the high-density jam above the second transition point, $p > p_t$, the diagonal correlation decays. The exponent β for the short-range correlation increases in proportion to the density p in the high-density region. The values of the exponent hardly depend on the system size. The values of the exponent themselves, however, seem not to be meaningful for the high-density region, because they depend on the value of ϵ in Eq. (4.3).

The diagonal correlation can be fitted also with exponential functions $\tilde{C}_{dd}^{\mathrm{diag}}(r) \propto \exp(-r/\xi)$ for large r. The correlation length ξ exceeds the system size N in the low-density jam region (Fig. 9). This causes a power-law dependence of the diagonal correlation. The correlation length suddenly decreases to $\xi \ll N$ near the transition point p_t. The estimated correlation lengths contain errors due to statistical errors and finite-size effects especially in the high-density jam phase.

V. STABILITY OF THE JAM

Finally, we investigate the difference of stability of the jam configurations in both phases mentioned above. To this end, we perturb the jam state to study the stability of the phase after the jamming state appears. In the center of jams, there are blockade pairs with an up arrow blocking the head of a right one or a right arrow blocking an up one. To perturb the jam phase, we remove one of such blockade pairs to the tail end of the jam leaving a pair of vacant sites in the center of the jam. Then the jamming state melts using these vacant sites. All cars stop again after some steps t in units of a cycle of traffic lights. We observe the distribution $P(t)$ defined as

$$P(t) = \frac{n(t)}{\sum_{t=0}^{\infty} n(t)}, \tag{5.1}$$

where $n(t)$ is the number of events affected by the perturbation until time t.

Let us briefly describe the actual simulation in the model to estimate the distribution $P(t)$. For the given values of N and p, we first give an initial random state using an adequate pseudorandom number generator. Starting from this state the system runs until a jam occurs. Then the perturbation mentioned above is applied, namely, removing a randomly chosen blockade pair to the tail end of the jam. For example, we consider the case that a blockade is a pair of a right arrow on the (i, j) site and an up arrow on the $(i+1, j)$ site. Then we start to find an empty site by moving leftward from the left-nearest site to the right-next-nearest of the (i, j) site. If the $(i-k, j)$ site is empty, it is marked as a destination candidate for the right arrow on the (i, j) site to move to. The same procedure is applied also to the up arrow on the $(i+1, j)$ site, searching for an empty site downward and marking a candidate. If a pair of vacant sites is

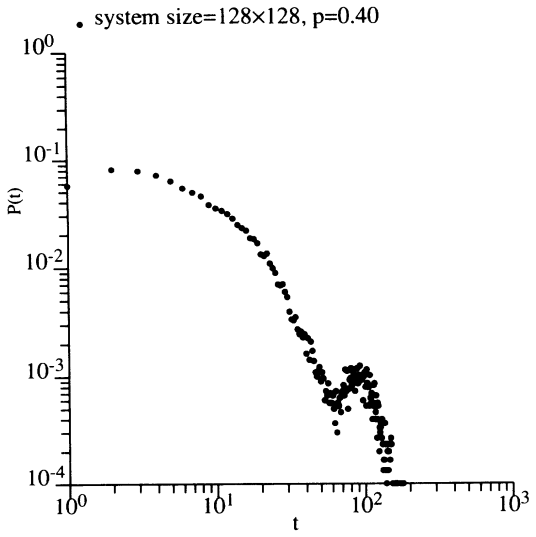

FIG. 10. The distribution $P(t)$ at $p \sim 0.4$ and $N = 128$. The data correspond to the summary of three runs; one run means 10 000 data points as mentioned in the text. The distribution has a peak corresponding to the system size.

marked as the destination, each one of the blockade pair is removed to the marked sites. If there is no available pair of empty sites, an attempt is made to find another blockade pair for removing. After removing a blockade pair, the system runs until the next jam occurs. Then the next perturbation is given. For one initial random state, 10 000 such perturbations are applied repeatedly. These 10 000 data points are obtained in one run of the simulation. The detailed method of removing a blockade pair would not affect the results qualitatively.

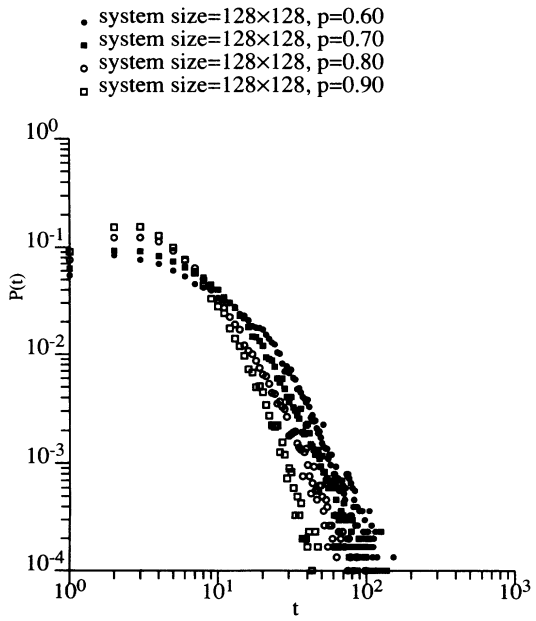

FIG. 11. The distribution $P(t)$ at $p > 0.6$ and $N = 128$. Each data point corresponds to the summary of three runs, one run means 10 000 data points as mentioned in the text.

The distributions $P(t)$ in the low-density jam are shown in Fig. 10. The effect of the perturbation remains for a long time. It propagates along the sequences of blockade pairs which compose the center of the jam. So the distribution $P(t)$ has a peak corresponding to the system size (Fig. 10).

In the high-density jam (Fig. 11), on the other hand, the effect of the perturbation vanishes in shorter times than the low-density cases. The distribution $P(t)$ decays in the large t region. The decay rate of $P(t)$ is not clear at this stage.

VI. DISCUSSION

We studied the properties of jams in a two-dimensional cellular-automaton model of traffic flow. The basic model treated here is the same as model I of Biham, Middleton, and Levine [8]. We found two types of jam (Fig. 12). At low density above the transition ($p_c < p < p_t$), a spatially diagonal long-range correlation appears. The backbone of the jam, sequences of blockade pairs, lies diagonally through the whole system. The branches of the jam spread horizontally and vertically. Thus the jam configurations are well organized. We call this type of jam a *self-organized jam.* In the high-density jam ($p > p_t$), on the other hand, local clusters of the jam cover the whole system and no global structure remains. We call this type of jam a *random jam.*

The spatial correlations were studied to characterize these two types of jam configurations. The spatially diagonal correlation obeys a power law in the low-density jam. Spatial correlations decay with increasing density. We defined the short-range exponent of the diagonal correlation for the high-density jam. The transition point p_t could be defined by the change in the values of the exponent.

The long-range diagonal correlations decay exponentially, reflecting the randomness of the system. The correlation length ξ exceeds the system size N in the low-density jam phase ($p < p_t$). It is expected that the correlation length remain finite in the $N \to \infty$ limit. We, however, have no clear evidence of the finite correlation length in the limit. Another possibility is that the cor-

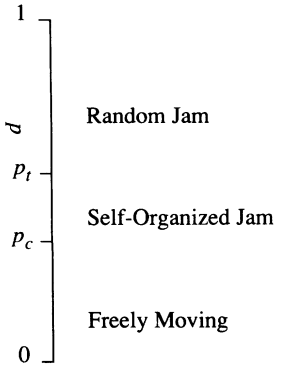

FIG. 12. Schematic phase diagram of two-dimensional traffic flow model as a function of density p.

relation length diverges in the thermodynamic limit. In this case, it is expected that the two transition points p_c and p_t coincide with each other, and the low-density jam phase will be observed only just at p_c.

The stability of these jam configurations was investigated by applying perturbations to the jam configurations. We investigated the distribution $P(t)$ of the time that the effect of the perturbation remains. The distribution $P(t)$ at low density above the transition has a peak corresponding to the system size, reflecting the long-range correlation. Detailed analysis of the distribution $P(t)$ is discussed elsewhere.

The power-law relations of the diagonal correlation remind us of the self-organized critical properties of the jam configurations [14]. The jam configurations seem to be self-organized well in the low-density jam. At high density, however, the initial randomness remains and thus the jam configurations are not self-organized. We have no explanation for the origin of the power law and the values of the exponent at present.

The occurrence of the jam may be affected by boundary conditions and isotropy especially at low density. The effect of anisotropy ($p_{\rightarrow} \neq p_{\uparrow}$) has been studied by Nagatani [13]. He pointed out that strong anisotropy prevents the system from jamming. The effect of another isotropy is still unclear; namely, the effect of equality of the horizontal and vertical system sizes.

Cellular-automaton models of traffic flow are not restricted to traffic flow problems. They are simplified abstract models of exclusion processes. In one-dimensional models analogies to ballistic deposition have been found [8,15–17]. Although any connection of the two-dimensional models to physical systems has not been discussed so far, studies on these systems are expected to clarify behaviors of complex systems.

ACKNOWLEDGEMENT

The authors would like to thank T. Nagatani for sending us his articles.

[1] S. Wolfram, Rev. Mod. Phys. **55**, 601 (1983).
[2] K. Nagel and M. Schreckenberg, J. Phys. I (France) **2**, 2221 (1992).
[3] K. Nagel and H. J. Herrmann, HLRZ Report No. 46/93, 1993 (unpublished).
[4] A. Schadschneider and M. Schreckenberg, J. Phys. A **26**, L679 (1993).
[5] S. Yukawa, M. Kikuchi, and S. Tadaki, J. Phys. Soc. Jpn. (to be published).
[6] T. Musha and H. Higuchi, Jpn. J. Appl. Phys. **15**, 1271 (1976).
[7] M. Takayasu and H. Takayasu, Fractals **1**, 860 (1993).
[8] O. Biham, A. A. Middleton, and D. Levine, Phys. Rev. A **46**, 6124 (1992).
[9] J. A. Cuesta, F. C. Martínez, J. M. Molera and A. Sánchez, Phys. Rev. E **48**, 4175 (1993).
[10] T. Nagatani, J. Phys. Soc. Jpn. **62**, 1085 (1993).
[11] T. Nagatani, Physica A **198**, 108 (1993).
[12] T. Nagatani, Phys. Rev. E **48**, 3290 (1993).
[13] T. Nagatani, J. Phys. Soc. Jpn. **62**, 2625 (1993).
[14] P. Bak, C. Tang, and K. Wiesenfeld, Phys. Rev. Lett. **59**, 381 (1987); Phys. Rev. A **38**, 364 (1988).
[15] P. Meakin, P. Ramanlal, L. M. Sander, and R. C. Ball, Phys. Rev. A **34**, 5091 (1986).
[16] J. Krug and H. Spohn, Phys. Rev. A **38**, 4271 (1988).
[17] S. A. Janowsky and J. L. Lebowitz, Phys. Rev. A **45**, 618 (1992).

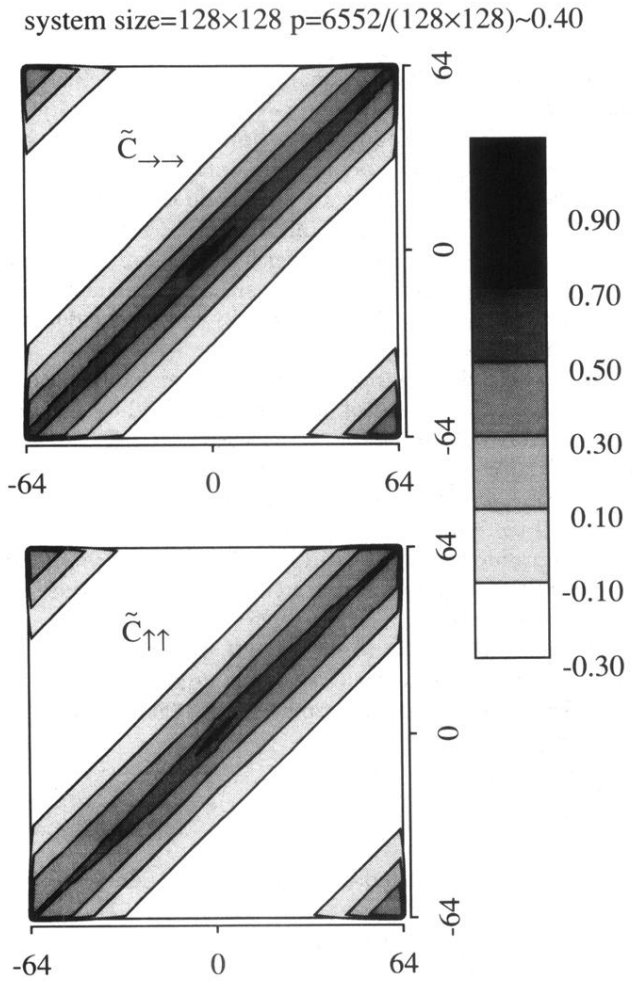

FIG. 3. The normalized correlation functions $\tilde{C}_{dd}(\vec{r})$ at low density. The upper diagram is of $\tilde{C}_{\rightarrow\rightarrow}(\vec{r})$ and the lower $\tilde{C}_{\uparrow\uparrow}(\vec{r})$. The correlation spreads diagonally over the system size. The high-value regions at the upper-left and lower-right corners are caused by finite-size effects. The system size is 128×128 and the density $p = 6552/(128 \times 128) \sim 0.4$. The average is taken over ten samples.

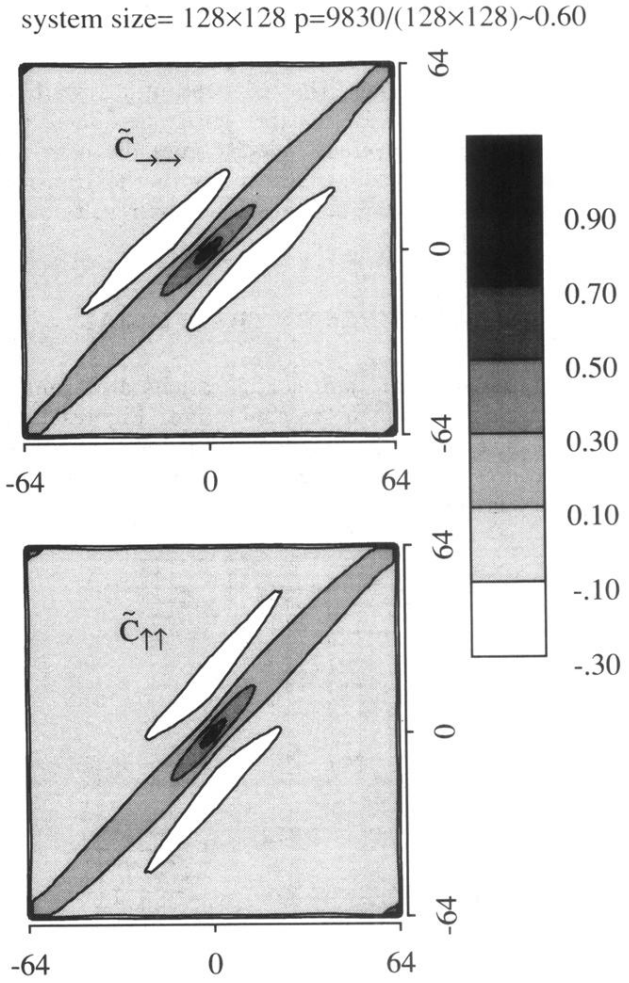

FIG. 4. The normalized correlation functions $\tilde{C}_{dd}(\vec{r})$ at intermediate density. The upper diagram is of $\tilde{C}_{\rightarrow\rightarrow}(\vec{r})$ and the lower $\tilde{C}_{\uparrow\uparrow}(\vec{r})$. The correlation mainly spreads diagonally over the system size. There appears a vibration in the antidiagonal direction in contrast to the low-density jam. The system size is 128×128 and $p = 6552/(128 \times 128) \sim 0.4$. The average is taken over ten samples.

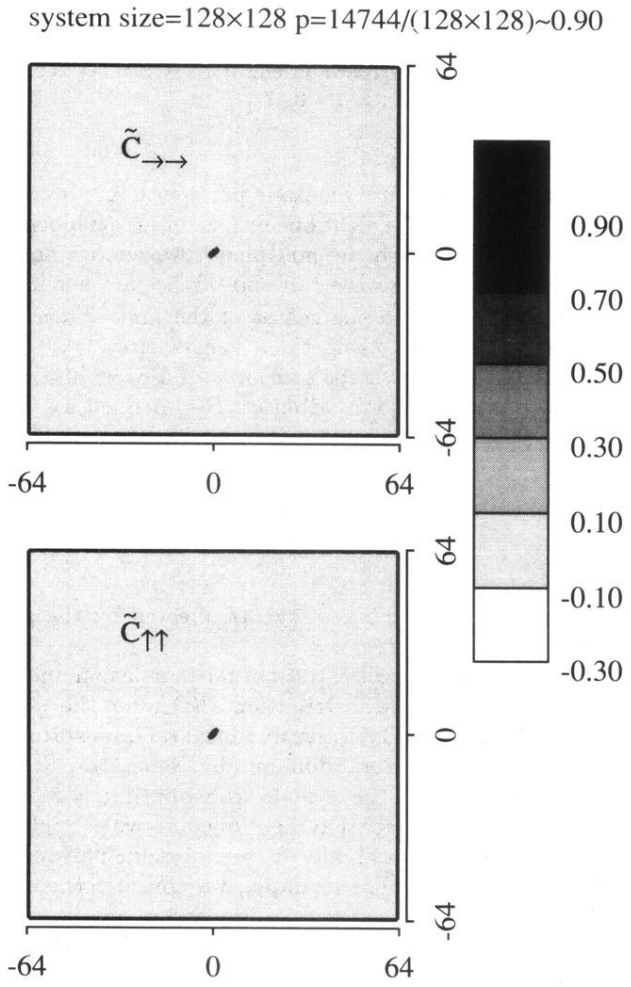

FIG. 5. The normalized correlation functions $\tilde{C}_{dd}(\vec{r})$ at high density. The upper diagram is of $\tilde{C}_{\rightarrow\rightarrow}(\vec{r})$ and the lower $\tilde{C}_{\uparrow\uparrow}(\vec{r})$. The values of $\tilde{C}_{dd}(\vec{r})$ are almost zero over the whole region except in the vicinity of the coordinate origin. The system size is 128×128 and $p = 14744/(128 \times 128) \sim 0.9$. The average is taken over ten samples.